Cranked Nilsson-Strutinsky vs the spherical shell model: A comparative study of *pf*-shell nuclei

Andrius Juodagalvis,[1] Ingemar Ragnarsson,[2] and Sven Åberg[2]
[1]*Institute of Theoretical Physics and Astronomy, A. Gostauto St. 12, LT-01108 Vilnius, Lithuania*
[2]*Mathematical Physics, Lund Institute of Technology, P.O. Box 118, S-22100 Lund, Sweden*
(Received 19 February 2005; published 28 April 2006)

A comparative study is performed of a deformed mean field theory, represented by the cranked Nilsson-Strutinsky (CNS) model and the spherical shell model. Energy spectra, occupation numbers, $B(E2)$ values, and spectroscopic quadrupole moments in the light *pf*-shell nuclei are calculated in the two models and compared. The result is also compared to available experimental data which are generally well described by the shell model. Although the Nilsson-Strutinsky calculation does not include pairing, both the subshell occupation numbers and quadrupole properties are found to be rather similar in the two models. It is also shown that "unpaired" shell model calculations produce energies similar to those from the CNS. The role of the pairing energy in the description of backbending and signature splitting in odd-mass nuclei is also discussed.

DOI: 10.1103/PhysRevC.73.044327 PACS number(s): 21.10.Ky, 21.60.Cs, 21.60.Ev, 27.40.+z

I. INTRODUCTION

A large number of models have been developed to gain insight into the spectroscopic properties of nuclei. Two of the most successful models are the spherical shell model and the deformed shell model. Large-scale spherical shell model calculations provide excellent agreement with observed data, but less transparent physics interpretations. The deformed shell model, on the other hand, is a mean field approach that is more illustrative but gives less accurate agreement with data. A parallel study using the two models allows a better understanding of the underlying nuclear processes. In this paper, we aim at comparing the predictions of the spherical shell model (SM) with those of one version of the deformed shell model, namely, the configuration-dependent cranked Nilsson-Strutinsky (CNS) approach.

For nuclei in the mass region $A \sim 40$–50, with valence particles occupying *pf*-shell orbits, well-tested shell model calculations are available, see [1] and references therein. Nuclei in this region show several interesting collective phenomena, such as the existence of rotational bands, backbending of the yrast band, band termination, and the appearance of superdeformed as well as axially asymmetric shapes (triaxiality) [2–4]. Other interesting features which have been discussed for these nuclei are the role of isoscalar and isovector pairing [1,5], violation of SU(3) symmetry [6,7] and appearance of the "quasi-SU(3)" symmetry [8], violation of isospin symmetry [9,10], angular momentum dependence of the mirror energy difference [11–13], and Jacobi shapes [14]. This long but by no means complete list indicates the significant attention that these nuclei have received in the last few years.

Though both the spherical shell and the CNS models provide a microscopic description of a nucleus, they are basically different. One difference is that the shell model gives a laboratory frame description, while the CNS provides a description in the intrinsic frame of reference. Another difference is in the "model space" and the treatment of the nuclear interaction. Within the restricted model space of the spherical shell model, the residual interaction between the valence particles is completely taken into account. The deformed shell model uses a virtually unrestricted model space. However, only specific parts of the nuclear interaction are included, in particular the quadrupole-quadrupole interaction. Furthermore, the inclusion of this interaction is made in the mean field approximation, with the self-consistency condition treated in an approximate way through the Strutinsky energy theorem [15]. Comparing the two models allows us to identify, on the one hand, the missing parts of the nuclear interaction as well as correlations beyond the mean field in the deformed shell model and, on the other hand, model space limitations in the spherical shell model.

The development of the shell model computer code ANTOINE [16] led to extensive and rather systematic theoretical investigations of the lower part of the *pf* shell, see Refs. [1,2] for a review. These calculations resulted in a detailed understanding of the spectroscopy in this region of nuclei and have inspired much experimental work. The (unpaired) cranked Nilsson-Strutinsky model [17,18] has been applied to nearly all nuclei in the periodic table for which high-spin states have been studied. The model successfully describes terminating rotational bands, superdeformed bands, and the phenomenon of shape coexistence, see Refs. [18–20] and references therein. This model has also been used to describe a few nuclei in the region of the present study. The interpretation of selected high-spin data in ^{47,48,49}Cr and ^{47}V was discussed in Refs. [18,21], while the odd-odd nuclei ^{46}V and ^{50}Mn were investigated in Ref. [22].

The spherical shell model was previously compared to the mean field models for some nuclei in the $A \approx 40$ region [2,21–24], and a striking similarity in the predictions was found. In this paper we make additional comparisons between the CNS and the shell model. Backbending, the role of pairing, and its contribution to signature splitting are stressed. We shall concentrate on the *pf*-shell nuclei close to the $N = Z$ line with mass numbers between $A = 44$ and 49. By making a

more systematic comparison of the two models, we want to improve our understanding of the deformed mean field model, test its validity for fairly light nuclei, and, in particular, to gain a better understanding of the physical picture behind observed properties in the region. This will allow us to assess the reliability of the CNS approach in heavier nuclei, where spherical shell model calculations are not feasible at present.

The paper is organized in the following way. First, we describe the models in Sec. II. Predictions of the two models are confronted and compared in Sec. III. The study is summarized in Sec. IV.

II. MODELS

A. The shell model and the cranked Nilsson-Strutinsky model

Shell model results are calculated using the computer code ANTOINE [16]. Valence particles, occupying orbits in the full *pf* shell, interact via the residual interaction KB3 [25]. For quadrupole properties, effective charges $e_p = 1.5\,e$, $e_n = 0.5\,e$ are used. Most of the results obtained with a "complete" interaction have already appeared in the publications by the Madrid-Strasbourg group (for a recent review see Ref. [1]). Here we will also present "unpaired" calculations which have not been presented before. The nucleus ^{48}Cr has been discussed using different values of the pairing strength [26].

CNS calculations are performed utilizing the modified oscillator potential and a standard set of parameters [17,18]. The implementation allows us to minimize the energy for a fixed configuration at a given value of the total angular momentum with configurations defined as explained in Refs. [18,27]. The total energy is minimized by varying three degrees of freedom: Two quadrupole parameters, ε (deformation) and γ (nonaxiality), and one hexadecapole parameter ε_4 [17]. Since all kinds of pairing interactions are neglected, the CNS results are mainly valid at high spin, and it becomes natural to normalize experimental and calculated energies at some high spin value. However, since some pairing may also remain at the highest spin states, we normalize the unpaired CNS energies to the calculated *unpaired* shell model energies at high spins. This is contrary to the spherical shell model where the corresponding normalization to experiment is generally done at the ground state. The same normalization energy is also subtracted from the unpaired shell model energies.

The calculated energies are often plotted with a subtracted rotational reference $E_{\rm ref} = 32.32A^{-5/3}I(I+1)$ MeV [18] in order to facilitate reading the figures and to highlight differences relative to this smooth rotational behavior. The reference corresponds to the rotation-energy of a rigid rotor for a prolate nucleus with a radius constant $r_0 = 1.20$ fm and a deformation $\varepsilon \approx 0.23$.

B. Moments

A translation between the intrinsic frame of reference and the laboratory frame of reference can be obtained using the rotor model, where those two frames can be related, see [28]. Thus, having values of the quadrupole deformation parameters ε and γ, it is possible to estimate the strength of the $E2$ transition between the two states, $B(E2)$, and the spectroscopic quadrupole moment of a state $Q_{\rm spec}$. And vice versa, using the values of $B(E2)$ and $Q_{\rm spec}$, the quadrupole deformation of a nucleus can be derived. Formally, this identification is valid only for fixed, axially symmetric shapes.

In the CNS approach, we calculate the intrinsic quadrupole moments from proton single-particle wave functions at appropriate equilibrium deformations. Neutrons have no contribution to this moment. Since the rotor model assumes an axially symmetric shape, while the calculated triaxiality parameter is usually sizable, we use an approximate relation between the intrinsic moments and the laboratory-frame observables [21]. If a nucleus has a rather flat energy surface, quantum fluctuations may become important. To show their effect, we utilize an approximative method [21] in a few selected cases to add the effect of quantum fluctuations on calculated quadrupole properties.

C. Occupation numbers

Single j-shell occupation numbers are readily obtained from the shell model wave-function. In the CNS calculations, the eigenstates are expanded in a stretched basis. It is, however, straightforward to make a transformation into a spherical basis and then to add up the fractions of the spherical subshells of the eigenstates at the equilibrium deformations. The method is outlined in Ref. [29].

D. Pairing

The shell model includes all kinds of correlations, an important part of which is pairing. To investigate the effect of the pairing interaction, we perform two calculations: One using the complete interaction, and another using the interaction with the pairing force subtracted. As defined in Ref. [26], the pairing energy is the difference between the energies obtained in these two calculations. We consider both the isoscalar (np; $J = 1$, $T = 0$) and the isovector ($nn + pp + np$; $J = 0$, $T = 1$) $L = 0$ pairing [26,30]. Thus three kinds of pairing energy are discussed: $T = 0$ pairing energy, which is deduced from the interaction with a subtracted $T = 0$ pairing force; $T = 1$ pairing energy, which is deduced from the interaction with a subtracted $T = 1$ pairing force; and the total pairing energy, which is deduced from the interaction with both pairing forces subtracted. The normalized pairing force is defined as [30] $H_{\rm pair} = G_{\rm pair}\bar{P}^\dagger\bar{P}$. Using the values from Table I in Ref. [30] and $\hbar\omega_0 = 9$ MeV, the following strengths are obtained: $G_{T=0} = -(\hbar\omega/\hbar\omega_0)|E^{10}| = -0.51\hbar\omega$ and $G_{T=1} = -(\hbar\omega/\hbar\omega_0)|E^{01}| = -0.32\hbar\omega$, where $\hbar\omega = 40A^{-1/3}$ MeV. Since the CNS approach does not include the pairing interaction, it is reasonable to compare its predictions to the unpaired energies of the shell model. Note, however, that the unpaired shell model contains other types of correlations beyond the mean field approximation that underlies the CNS approach.

III. RESULTS

We compare the two models for even-even systems in Sec. III A, where the nuclei $^{44,46}_{22}$Ti and $^{48}_{24}$Cr are discussed. For ^{48}Cr, the negative-parity band is discussed in addition to the ground-state band. This band has the largest negative γ deformation in the region. A few selected odd-even nuclei (namely, $^{45}_{22}$Ti, $^{47}_{23}$V, and $^{49}_{24}$Cr) are discussed in Sec. III B.

A. Even-even nuclei

1. *Positive-parity band in* ^{48}Cr

The nucleus ^{48}Cr has a half-filled $f_{7/2}$ shell of protons and neutrons, resulting in the largest ground-state deformation in the $f_{7/2}$ region. The yrast band shows an interesting behavior, being rotorlike with a backbend and a well-established termination at $I = 16^+$. It has been interpreted as having a triaxial shape [21,23]. The pairing energy along the band as well as quadrupole properties have been studied extensively [6,23,26,31–35]. This band is, therefore, a good example with which to start this broader comparison between the CNS and the shell model.

An exploratory study of ^{48}Cr using the CNS and shell model approaches [21] suggested that the predicted quadrupole properties are similar, although energies are rather different, see Fig. 1. (A similar conclusion was reached using the cranked Hartree-Fock-Bogolyubov (CHFB) method [7,23].) We continue this comparison particularly emphasizing the role of the pairing interaction. As in previous studies, we concentrate on the yrast positive-parity even-spin states between $I = 0$ and 16.

Since pairing is neglected in the CNS calculation, Fig. 1(a) also shows energies of two unpaired shell model calculations. The change in the smoothness of excitation energies suggests that the backbending behavior is mainly caused by the $T = 1$ pairing (as pointed out in Ref. [26] and further discussed in Ref. [33]), while the $T = 0$ pairing is generally smaller than the $T = 1$ pairing and decreases smoothly with spin. Small irregularities in the spin dependence of the $T = 0$ pairing energy enhance the trends in the $T = 1$ pairing energy. To see the backbending behavior better, we show the angular momentum vs the rotational frequency, $\hbar\omega(I) = [E(I) - E(I-2)]/2$, in Fig. 1(b). The complete shell model energies (as well as the experimental energies) show a rather strong backbending at $I \approx 12$. It becomes smaller if the $T = 1$ pairing is subtracted. The upbending is also seen in the CNS calculation. It is caused by the deformation change, see Fig. 2.

When the CNS energies are normalized to match the shell model excitation energy of a fully aligned state at $I = 16^+$, they fall between the two unpaired shell model energies: With only the $T = 1$ pairing subtracted and the pairing interaction removed completely [Fig. 1(a)]. However, they come much closer to the shell model results without the $T = 1$ pairing. A similar behavior was noted in Ref. [23], where the shell model and CHFB calculations were compared. This deviation of the CHFB results from experiment was attributed to the improper treatment of the proton-neutron pairing by the latter mean field method [7,23].

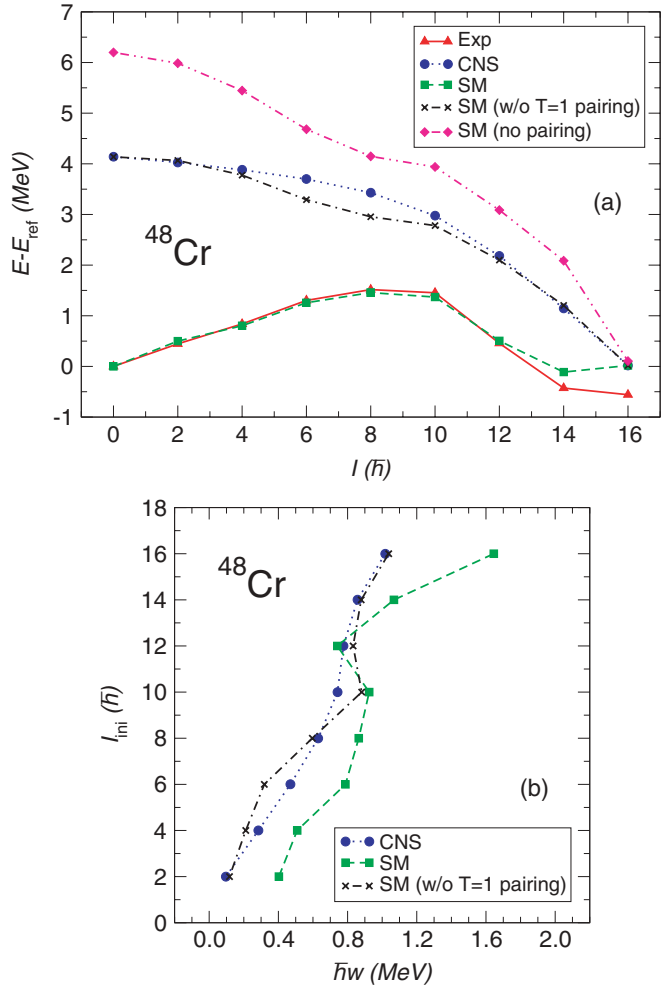

FIG. 1. (Color online) Energies in the ^{48}Cr yrast band plotted (a) relative to a rotational reference and (b) as the total angular momentum vs the rotational frequency (backbending plot). Experimental values [32] are shown by triangles. Results of four calculations are also shown: CNS, complete shell model, and two unpaired shell model cases, one without the $T = 1$ pairing and one without both the $T = 0$ and the $T = 1$ pairing. Calculated CNS energies in (a) are matched to the shell model excitation energy of the fully aligned 16^+ state.

We already noted the similarity of the quadrupole properties as described by the two approaches [21] and will discuss them more below. Here we would like to point out that a more detailed investigation of the results shows that the calculated wave functions are similar as well. The spherical j shells are occupied almost identically, see Fig. 3. In particular, there is a very good agreement in the occupation of the $f_{7/2}$, $p_{3/2}$ and $p_{1/2}$ shells, despite the fact that the two models treat the model space in a different manner; moreover, pairing as well as other correlations beyond the mean field are completely neglected in the CNS. The effects of the $T = 1$ pairing interaction are visible in the increased occupation of the $f_{5/2}$ shell and the decreased occupation of the $f_{7/2}$ shell. This is easily understood in the BCS picture of the $T = 1$ pairing. The pairing causes occupations of orbitals around the Fermi surface

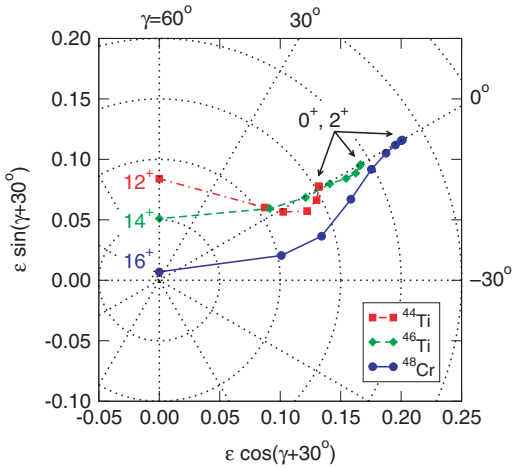

FIG. 2. (Color online) CNS calculated equilibrium deformations along the yrast bands in three even-even nuclei. Deformation change between the $I = 0$ and $I = 2$ states is negligible in all these nuclei.

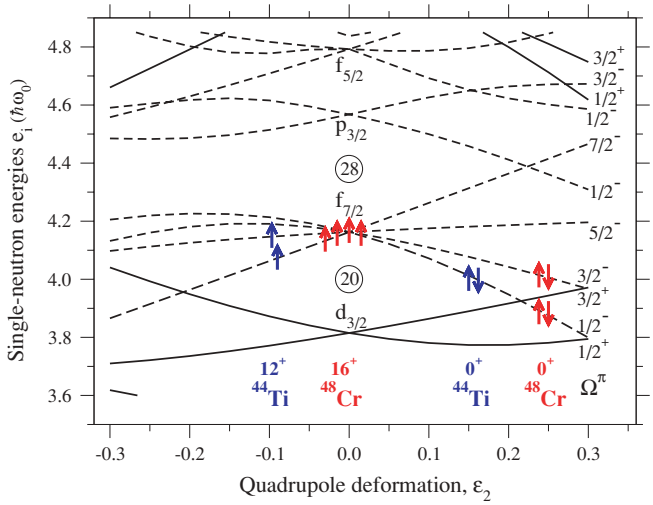

FIG. 4. (Color online) Nilsson diagram for single-neutron states in the modified oscillator potential. Arrows symbolize particles; their direction indicates whether m_j is positive (arrow up) or negative (arrow down). The ground state as well as the band-terminating state with all particles in the $f_{7/2}$ shell are shown for ^{48}Cr and ^{44}Ti.

to be smeared out; the Fermi surface in the nucleus ^{48}Cr is in the middle of the $f_{7/2}$ shell and below the $f_{5/2}$ shell.

The CNS predicts a much lower occupation of the $f_{5/2}$ shell (0.06 particles in the ground state as compared to 0.56 particles predicted by the shell model); in addition, some occupation is found outside the *pf* shell. The contents of excitations outside the spherical *pf*-shell model space decrease smoothly with spin from 0.28 particles in the ground state to zero in the band-terminating state. The general agreement in occupation numbers between the two models is remarkable, since partial occupancies of the spherical *j* shells have different origins in the two models. The two-body interaction between valence particles causes configuration mixing in the shell model. On the other hand, the mixing of spherical *j* shells is determined by the deformation and rotation in the CNS approach.

Equilibrium deformations calculated in the CNS model at different spin values are shown in Fig. 2 (note that a comparison with the CHFB results [23] is presented in Fig. 3 of Ref. [21]). The quadrupole deformation of the ground state, $\varepsilon \approx 0.23$, implies a fairly large mixing of the spherical $f_{7/2}$ and $p_{3/2}$ shells, see the Nilsson diagram in Fig. 4. Since all four positive *m* states of the $f_{7/2}$ subshell are occupied for protons as well as for neutrons in the band-terminating state 16^+ (cf. Fig. 3), the nucleus obtains a spherical shape. A gradual change in deformation, as spin increases from the ground state to the 16^+ state (Fig. 2), explains the main changes in the occupation numbers of the $f_{7/2}$ and $p_{3/2}$ shells, seen in Fig. 3. When the deformation decreases, the spherical *j* shells are less mixed.

The particular importance of the $f_{7/2}$-$p_{3/2}$ mixing in creating rotational motion, an example of "quasi-SU(3)" symmetry, was discussed by Zuker *et al.* [8]. This mixing originates from the quadrupole force that is a key part of the CNS. It is most interesting to note [8] that expectation values of the full shell model Hamiltonian in eigenstates of a pure *QQ* force give a backbending behavior of energies, i.e., they include the pairing features, while corresponding energies from the *QQ* force do not show backbending. This indicates, as found also in Fig. 3, that the wave functions of the CNS model are similar to those of the full shell model.

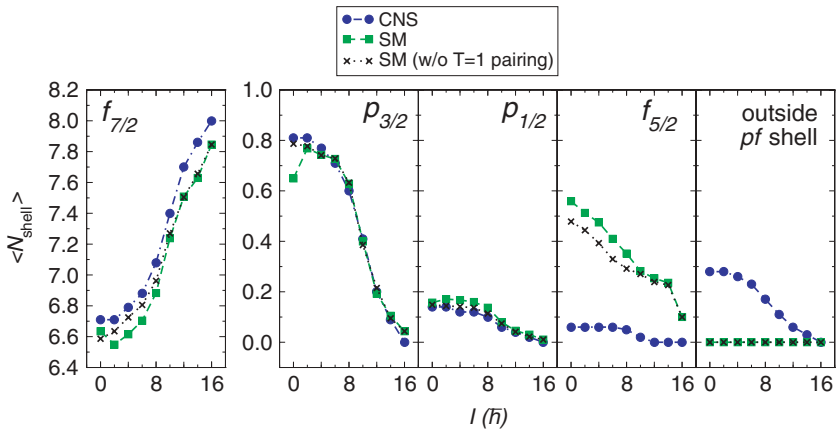

FIG. 3. (Color online) Average total number of particles (neutrons and protons) in the *spherical j* shells in ^{48}Cr.

2. *Negative-parity band in* ^{48}Cr

A negative-parity band in the *pf*-shell nuclei can be obtained by exciting one particle (a proton or a neutron) from a $d_{3/2}$ orbit to an unoccupied $f_{7/2}$ orbit, forming a configuration $d_{3/2}^{-1} f_{7/2}^{9}$. Depending on the signatures of the $d_{3/2}$ hole and the odd $f_{7/2}$ particle, eight configurations can be formed. Since the Coulomb interaction has a small effect, mirror configurations are almost identical. Out of the remaining four different bands, the lowest band in the CNS calculation has odd spins, and the bandhead is $K^{\pi} = 4^{-}$ (excitation $d_{3/2,3/2}^{-1} f_{7/2,5/2}$). The two even-spin bands, having $\alpha_{\rm tot} = 0$, are nearly degenerate and their equilibrium deformations are slightly different. Thus, we present only the bands with $\alpha(d_{3/2}^{-1}) = -1/2$.

The measured and the CNS energies of the negative-parity band in ^{48}Cr are shown in Fig. 5. Brandolini *et al.* [32] reported a shell model calculation with a $d_{3/2}$ hole included. The lower part of the spectrum could be well described, while higher spins were described poorly. These energies are not included in Fig. 5.

CNS predicts a slightly bigger moment of inertia than observed experimentally. This could be expected from the absence of pairing correlations in the model. The amount of pairing energy can be estimated, assuming that it originates from the *pf*-shell particles only. In this case, it would have a spin dependence similar to that in ^{49}Cr (see later in Fig. 16). The thus obtained approximate prediction of the unobserved energies in the negative-parity band is not shown in the figure. We note, however, that the contribution from the pairing correlations is expected to approximately double the signature splitting predicted by the CNS calculations shown in Fig. 5.

Calculated equilibrium deformations for the negative-parity bands are shown in Fig. 6. The 4^{-} bandhead has a similar deformation as the 0^{+} ground state, in agreement with the measured $B(E2)$ values [32,36]. However, already this state is triaxial. Nonaxiality gets stronger as spin increases, and the band terminates in a noncollective prolate shape ($\gamma = -120^{\circ}$).

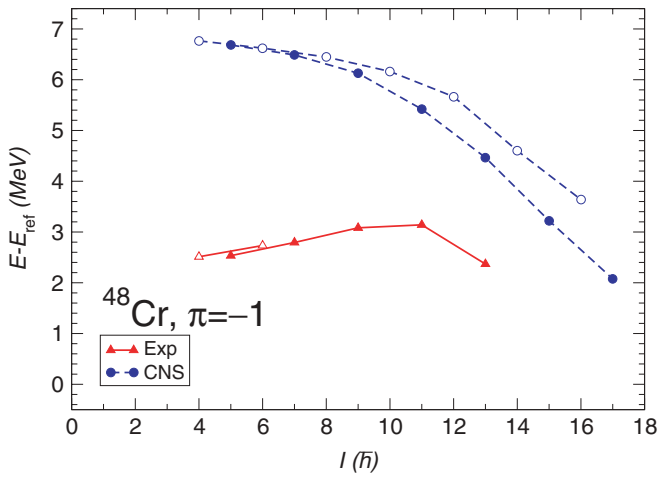

FIG. 5. (Color online) Energies of the negative-parity band in ^{48}Cr. Experimental data are from Ref. [32]. Filled and empty symbols differentiate between the $\alpha = 1$ and $\alpha = 0$ bands respectively. CNS energies are normalized in the same way as for the ground-state band in Fig. 1.

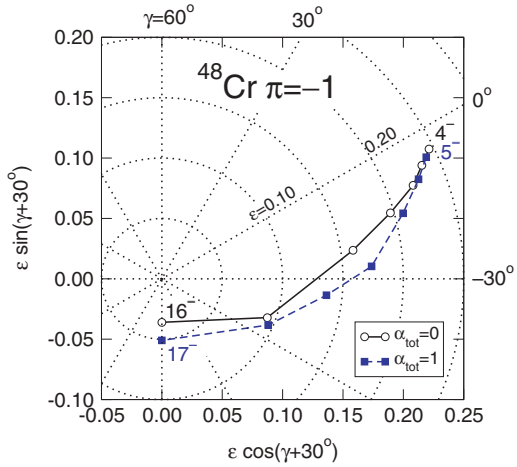

FIG. 6. (Color online) CNS-calculated equilibrium deformations in the ^{48}Cr negative-parity band. The odd particle in $f_{7/2}$ has $\alpha = +1/2$ for the even-spin states ($\alpha_{\rm tot} = 0$) and $\alpha = -1/2$ for the odd spins ($\alpha_{\rm tot} = 1$), while the $d_{3/2}$ hole has $\alpha = -1/2$.

In fact, this negative-parity band in ^{48}Cr exhibits the largest calculated negative-γ deformation in the region of *pf*-shell nuclei. This can be understood by analyzing single-particle Routhians, see later in Fig. 11. A hole in the $N = 2$, $\alpha = +1/2$ orbital, shown in the figure by a solid line, has a strong polarization effect toward negative γ values. The excited particle will occupy either the 25th or 26th orbital, which are both essentially γ independent. Thus, the net effect is a large negative-γ deformation of the bands. Since at high spins the spectroscopic quadrupole moment is proportional to $\sin(\gamma + 30^{\circ})$ [37], we expect it to be small in this band. The gradual decrease in ε deformation also causes the stretched $B(E2)$ values to decrease with increasing spin toward the band-terminating states at 16^{-} and 17^{-}.

3. *The nuclei* ^{44}Ti *and* ^{46}Ti

Calculated and experimental energies of the yrast states in ^{44}Ti and ^{46}Ti are compared in Fig. 7. These two nuclei have several measured bands (see Refs. [38] and [39], respectively) but we restrict ourselves to the yrast bands only. As expected from the neglect of pairing, the CNS energies deviate from experimental data at low spins. The shell model does not reproduce the ^{44}Ti spectrum excellently because excitations out of the *sd* shell play an important role in this nucleus [38].

In addition to the complete results, Fig. 7 shows two other shell model calculations: with only the $T = 1$ pairing subtracted, and with both pairings subtracted. Pairing does not contribute much at $I > 6$. This is particularly true for ^{44}Ti, where both the $T = 0$ and $T = 1$ pairing energy contributions are approximately zero. The CNS energies compare well with those unpaired calculations, especially with the one where only the $T = 1$ pairing is removed. This pairing is the main cause of backbending at $I \approx 10$ in both nuclei, since the energy contribution from the $T = 0$ pairing has a smooth dependence, decreasing with spin. All these features are similar to those in ^{48}Cr (Fig. 1).

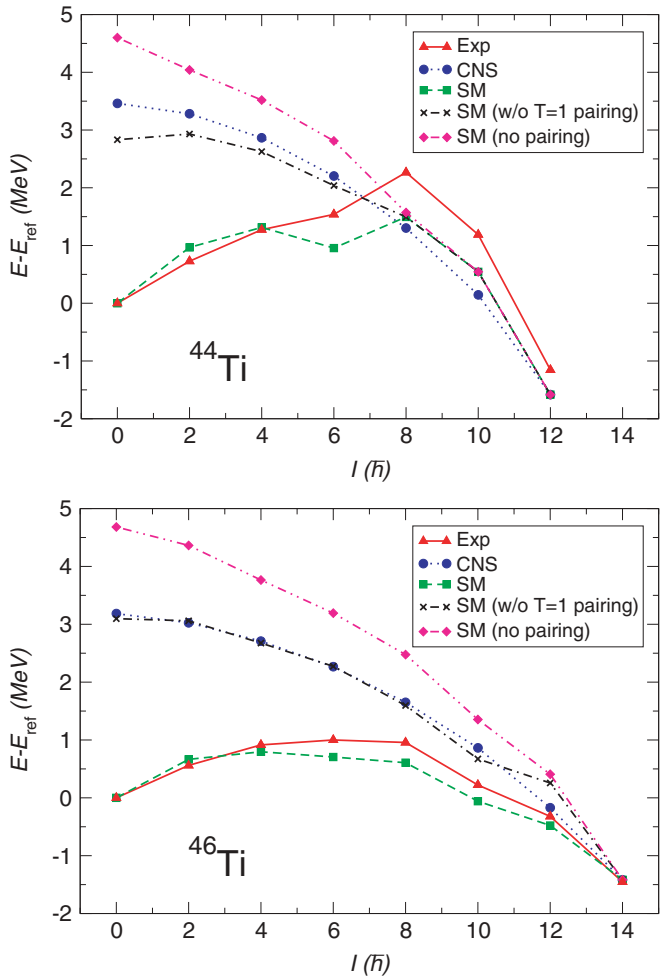

FIG. 7. (Color online) Excitation energies of the yrast states in ^{44}Ti and ^{46}Ti plotted relative to a rotational reference. Experimental energies in ^{44}Ti and ^{46}Ti are taken from Refs. [38] and [39], respectively.

Having half-filled $f_{7/2}$ shells for both protons and neutrons, the ^{48}Cr nucleus is the most collective nucleus in the region. Since the lower $f_{7/2}$ orbitals are deformation-driving (see the Nilsson diagram in Fig. 4), subsequent removals of a pair of protons (giving ^{46}Ti) and a pair of neutrons (^{44}Ti) reduce collectivity. The quadrupole deformations $\varepsilon = 0.23, 0.19$, and 0.15 are predicted for the ground states of the nuclei ^{48}Cr, ^{46}Ti, and ^{44}Ti, respectively, see the calculated equilibrium deformations shown in Fig. 2.

Available experimental information and the calculated $B(E2)$ values for the two titanium isotopes are shown in Fig. 8. Both the shell model and the CNS suggest a gradual decrease in collectivity as the angular momentum increases. The transition strengths are very similar in the two models, especially if the CNS results are corrected for quantum fluctuations around the equilibrium. Yrast bands terminate at $I = 12^+$ and 14^+ with some remaining collectivity: $B(E2; \text{exp}) \approx 4$ W.u.

B. Odd-even nuclei

In this section, we discuss odd-even mass nuclei with $N = Z \pm 1$. The nuclei having $A = 45$ and 47 are presented in Sec. III B1, while the results for ^{49}Cr are presented in Sec. III B2. The role of pairing in backbending as well as in signature splitting is discussed in Sec. III B3.

1. $A = 45$ and $A = 47$ nuclei

The mirror nuclei $^{45}_{22}\text{Ti}_{23}$-$^{45}_{23}\text{V}_{22}$ and $^{47}_{24}\text{Cr}_{23}$-$^{47}_{23}\text{V}_{24}$ have identical spectra in the shell model since the Coulomb and other isospin-nonconserving interactions are neglected in favor of a good isospin. In CNS, where protons and neutrons have different single-particle spectra because of the Coulomb interaction, the predicted properties of mirror nuclei are still very similar, because the effect of isospin-violating interactions is relatively small in this mass region: experimental mirror energy difference is below 100 keV [9,10,13]. Because of this similarity in spectra, we present the calculated results only for ^{45}Ti and ^{47}V.

Experimental and calculated energies of the yrast states in ^{45}Ti and ^{47}V are compared in Fig. 9. The signature $\alpha = +1/2$ levels in ^{45}Ti are known up to $I^\pi = 17/2^-$, and the energy

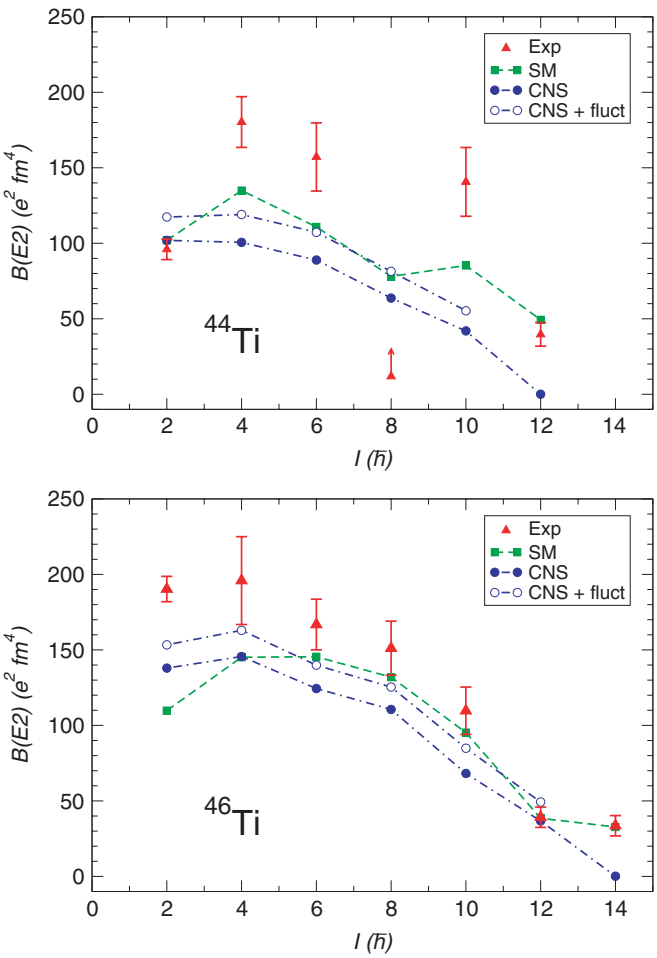

FIG. 8. (Color online) Strength of the stretched $E2$ transitions along the yrast bands of ^{44}Ti and ^{46}Ti. Measured values from Refs. [40,41] and [3], respectively. Empty circles show the CNS predictions taking into account quantum fluctuations around the equilibrium shape.

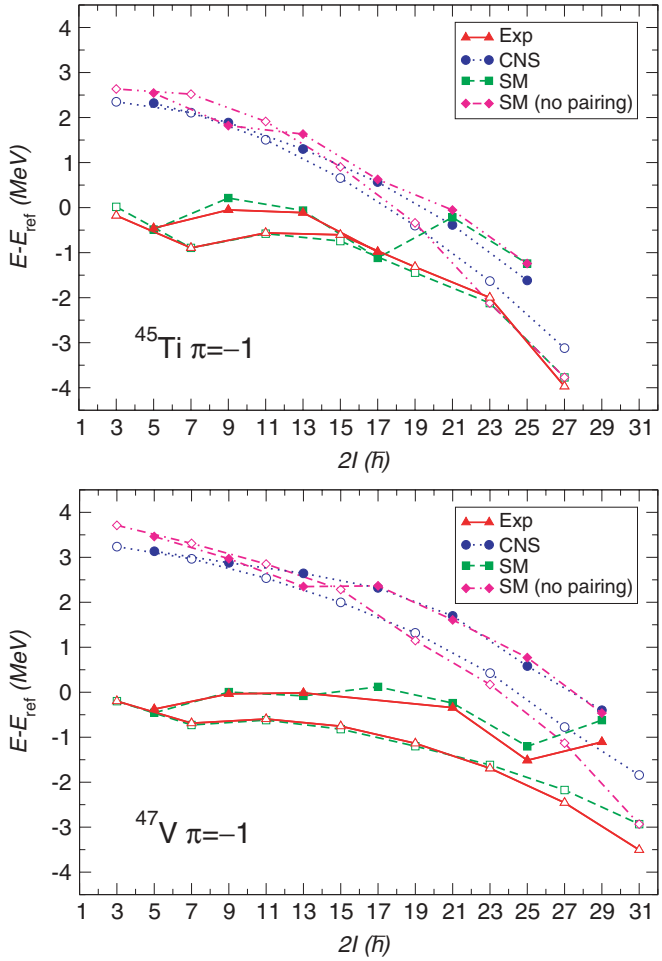

FIG. 9. (Color online) Energies of yrast states in ^{45}Ti and ^{47}V. Experimental data from Refs. [42] and [43], respectively. Levels $21/2^-$ and $25/2^-$ in ^{45}Ti and the $17/2^-$ state in ^{47}V are not known. Filled and empty symbols distinguish between $\alpha = +1/2$ and $\alpha = -1/2$ bands, respectively.

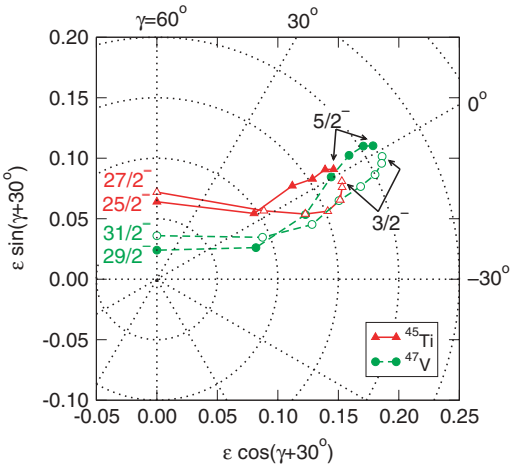

FIG. 10. (Color online) Equilibrium deformations along the yrast bands in odd-even nuclei ^{45}Ti and ^{47}V calculated in the CNS. Similar deformations are predicted for the mirror nuclei ^{45}V and ^{47}Cr, respectively.

of the $17/2^-$ level in ^{47}V is not measured. These missing levels inhibit discussion of the pair-alignment process in the backbending region, since the mirror energy difference cannot be extracted. Therefore, we discuss the behavior of the signature partners in a different way.

The ground states of ^{45}Ti and ^{47}V are described in the CNS with an odd particle occupying the $\Omega = 3/2$ state of the $f_{7/2}$ shell, see Fig. 4. This gives rise to a fairly large rotation-induced signature splitting which varies smoothly with angular momentum. The different character of the signature partners, observed experimentally in both nuclei, is thus expected to originate from the pairing force. This conclusion is supported by the good agreement between the unpaired shell model and the CNS energies (Fig. 9). Although the unpaired shell model energies show more structure than the CNS energies, the moments of inertia and the signature splittings are essentially the same in the two models. We expand the discussion of the role of pairing for the signature splitting in Sec. III B3.

Calculated equilibrium deformations for the two signature-partner bands in ^{45}Ti and ^{47}V are shown in Fig. 10. An interesting staggering of the shape is seen. The $\alpha = +1/2$ band has positive γ values, while its signature partner, the $\alpha = -1/2$ band, has negative γ values. The different γ deformations of the two signature bands affect the quadrupole properties, while energies are less sensitive to the small changes of the triaxiality parameter. The equilibrium deformations change smoothly from $\varepsilon = 0.17$ (0.21) in the ground state of ^{45}Ti (^{47}V) to $\varepsilon \approx 0.07$ (0.03) in the band-terminating state, having noncollective oblate shape ($\gamma = 60^\circ$). The values of the γ parameter do not exceed 10° for most of the states prior to termination.

This different γ preference may be understood from the single-particle Routhians plotted at fixed rotational frequencies in Fig. 11. The encircled numbers show the number of particles below that point. The 23rd single-particle orbital prefers either a positive or negative γ value, depending on whether the $\alpha = +1/2$ or $-1/2$ branch is occupied. This single-particle orbital is crucial to both $^{45}_{22}\mathrm{Ti}_{23}$ and $^{47}_{24}\mathrm{Cr}_{23}$, because neither the 22 protons in ^{45}Ti nor the 24 neutrons in ^{47}V have any strong preference in γ, as we discuss below. Since the single-neutron and single-proton level schemes are very similar, the same arguments apply for the $^{45}_{23}\mathrm{V}_{22}$ and $^{47}_{23}\mathrm{V}_{24}$ nuclei as well.

The Routhians of Fig. 11 can also be used to illuminate the triaxial properties of nuclei with N or Z equal to either 22 or 24. The summed effect of the two lowest $f_{7/2}$ orbitals (dashed and dash-dotted lines below particle number 22 in Fig. 11) gives no strong preference in the γ direction. The 23rd and 24th orbitals have forces driving in different γ directions, leading to opposite γ deformations which results in no γ sign preference for 24 particles. This is reflected in nearly axial deformation of the ground-state band in ^{48}Cr at low spins [21]. The highest $N = 2, \alpha = +1/2$ orbital has a strong γ driving force, which explains large negative-γ deformations in the 1p-1h bands, as in the case of the negative-parity band in ^{48}Cr, see Sec. III A2.

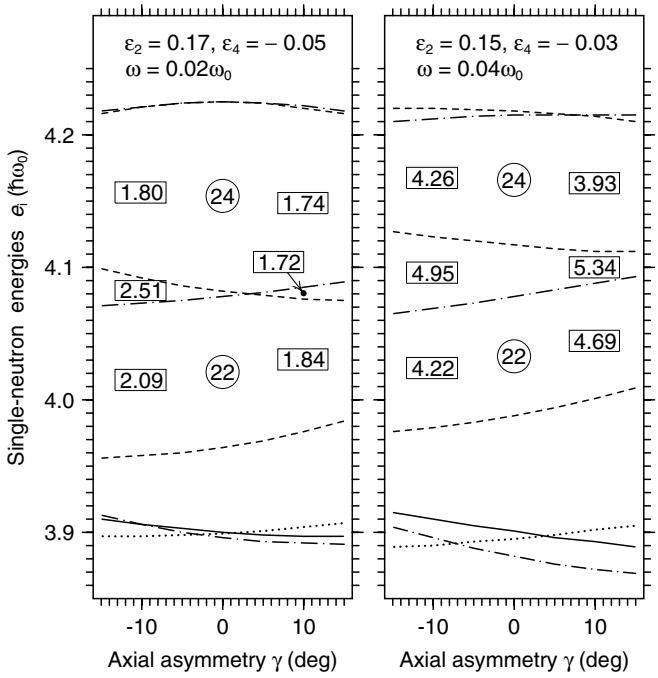

FIG. 11. Dependence of the single-particle Routhians on the nonaxiality parameter γ at deformations and rotational frequencies relevant for $I \approx 4$ (left panel) and $I \approx 8$ (right panel) states in ^{45}Ti. Encircled numbers indicate the number of orbitals below that point. Boxed numbers show the spin contributions from all 22, 23, and 24 neutrons at $\gamma \pm 10^{\circ}$. Positive-parity orbitals from the sd ($N = 2$) shell are drawn by solid ($\alpha = +1/2$) and dotted ($\alpha = -1/2$) lines. Other lines are negative-parity pf-shell orbitals: the $\alpha = +1/2$ orbitals, dashed lines, while the $\alpha = -1/2$ orbitals, dash-dotted lines. Diagram is drawn for neutrons, but proton orbitals show very similar properties.

2. *The nucleus* ^{49}Cr

Calculated and experimental yrast energies for ^{49}Cr are shown in Fig. 12. The observed splitting of the signature partners is small at low spins. However, at spin $I = 15/2$ the $\alpha = -1/2$ band changes its smooth behavior in a backbending.

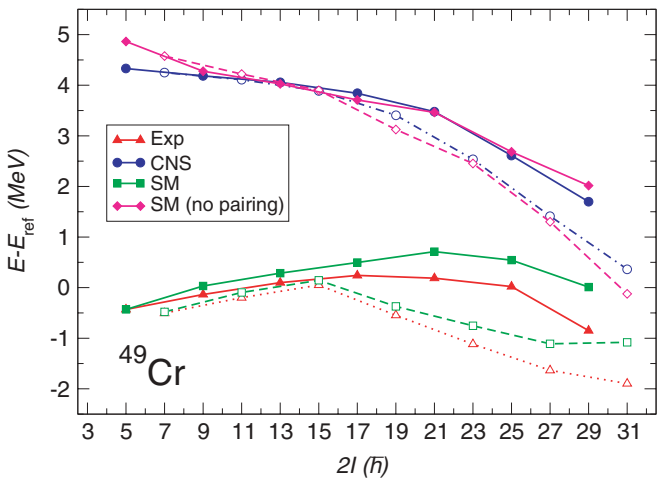

FIG. 12. (Color online) Experimental [43] and calculated energies of yrast states in ^{49}Cr.

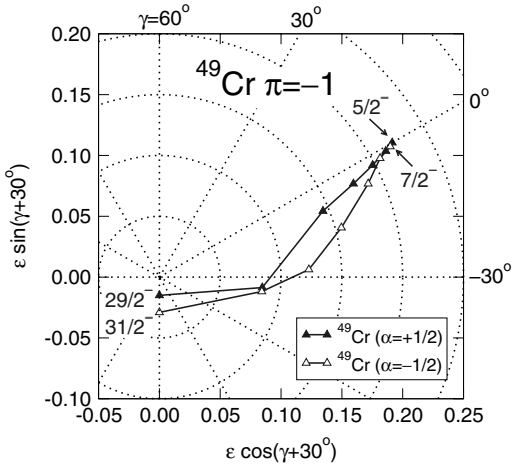

FIG. 13. CNS-predicted equilibrium deformations along the yrast band in ^{49}Cr.

The other signature band depends on angular momentum in a smoother way up to the band termination. This behavior of the two signature partner bands is well reproduced by the shell model [44], although there is a systematic deviation at higher spins. The CNS calculations show large deviations, particularly for low spins, as is expected from the lack of pairing correlations in this model. A rather small signature splitting originates from the odd neutron occupying the $\Omega = 5/2$ orbital of the $f_{7/2}$ shell. Similarly, as in the case of ^{45}Ti and ^{47}V, the shell model signature splitting reduces if the pairing interaction is removed. These energy values agree very well with the CNS calculation. The next section is devoted to exploring this observation.

Calculated equilibrium deformations in the lowest $\alpha = +1/2$ and $-1/2$ bands in ^{49}Cr are shown in Fig. 13. The spin dependence of the quadrupole deformation parameter ε was briefly discussed in Ref. [11]. Here we present a more detailed study. Both signature bands prefer negative γ values already at low spins. They terminate in noncollective prolate states ($\gamma = -120^{\circ}$) at spins $I^{\pi} = 29/2^{-}$ and $31/2^{-}$, respectively.

Based on the equilibrium deformations, the $B(E2)$ values and the spectroscopic moments Q_{spec} were calculated. They are shown in Fig. 14 together with experimental data on $B(E2)$ [43] and the shell model results. (No experimental information on spectroscopic quadrupole moments is available.) The agreement between the two model predictions is good. As spin increases, the nuclear shape gradually changes from axially symmetric prolate to triaxial shapes with negative γ values, see Fig. 13. Simultaneously, the quadrupole parameter ε gets smaller, which explains the gradual decrease of the $B(E2)$ values for both signatures. The Q_{spec} values are additionally reduced by γ approaching -30°. It is interesting to note that the quadrupole properties along the signature bands are similar, although the energies in one of them show a backbending behavior.

As discussed above, the shapes of both signatures in ^{49}Cr change with increasing spin and become clearly triaxial after spin $I > 17/2$, where the rotation takes place around the intermediate axis (indicated by a negative value of γ in the

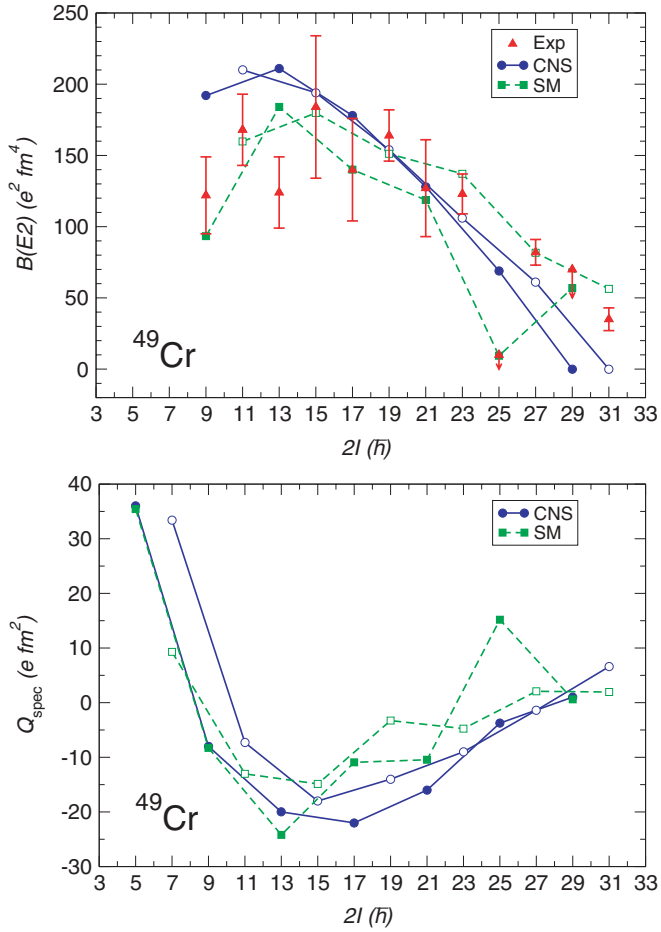

FIG. 14. (Color online) Quadrupole properties of yrast states in ^{49}Cr. Upper plot shows $B(E2)$ values for the stretched $E2$ transitions along the two signature bands. Experimental $B(E2)$ values are taken from Ref. [43]. Lower plot shows calculated spectroscopic quadrupole moments.

Lund convention). A signature of nuclear triaxiality in an odd-mass nucleus is the staggering of $B(E2; \Delta I = 1)$ values, as discussed by Hamamoto and Mottelson [37]. We plot them [43,45] in Fig. 15. It is clearly seen that the staggering in the shell model values of $B(E2; \Delta I = 1)$ indeed appears above the angular momentum $I = 17/2$, when the shapes calculated in the CNS become triaxial (Fig. 13).

3. *Pairing, Backbending and Signature Splitting*

Pairing correlations are the leading term beyond the mean field description. By removing either the $T = 1$ pairing force or both the $T = 0$ and $T = 1$ pairing forces from the shell model interaction, unpaired shell model energies could be obtained. Remarkably, these energies agreed very well with the energies calculated within the unpaired CNS model. This leads us to a more detailed study of the shell model pairing energy, its role in causing backbending of the ground-state band, and its contribution to the signature splitting.

In Fig. 16, we show separately the $T = 0$ and $T = 1$ pairing energies and their sum as a function of angular

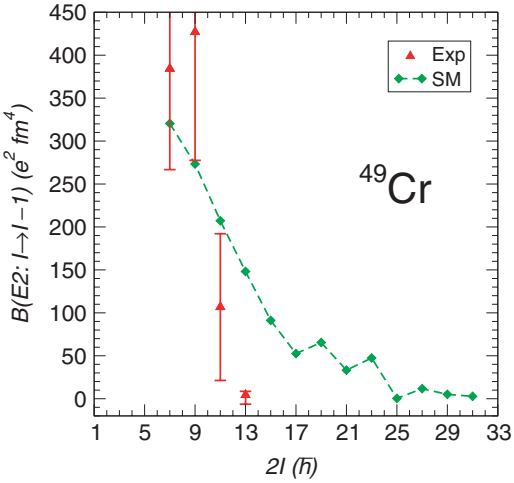

FIG. 15. (Color online) Unstretched $B(E2)$ values in ^{49}Cr: experimental data [45] and shell model predictions [43]. Staggering at higher spins indicates nonaxiality of the nuclear shape [37], as suggested by the CNS calculation (Fig. 13).

momentum for the three odd-even nuclei ^{45}Ti, ^{47}V, and ^{49}Cr. The $T = 0$ pairing energy behaves smoothly in a way similar to its behavior in the even-even nucleus ^{48}Cr (see Fig. 4 in Ref. [26]). Its contribution decreases from 1–2 MeV in the ground state to a small or zero contribution in the spin-aligned state (the highest angular momentum state shown in the figure). The $T = 1$ pairing shows a pronounced odd-even effect, see Fig. 17. The odd nucleon in the three studied odd-even nuclei implies a blocking effect that weakens the isovector pairing energy by about 1 MeV in the ground state, as compared to the neighboring even-even nuclei. The isoscalar pairing energy has a much smoother mass dependence. Note that the isoscalar pairing contributions seem to follow the same trend along the yrast band as the isovector pairing, although the irregularities are much smoother (Fig. 16).

The behavior of the isovector $T = 1$ pairing is easy to understand in terms of the seniority. To highlight the change of these pairing energies, we plot them separately in Fig. 18. The irregularities, seen in the $\alpha = -1/2$ signature band of the nucleus ^{47}V at $I = 7/2^-, 19/2^-$, and $27/2^-$, correspond to the maximum spin states in the single $f_{7/2}$ shell for seniorities $v = 1$, 3, and 5, respectively. These irregularities are more prominent in the $\alpha = +1/2$ band. However, they are shifted downward by one unit of angular momentum. Similar features are seen in the other nuclei, while the collectivity affects them and can even make them disappear.

As we shall see, the changes of the pairing energy with increasing spin causes backbending. Backbending of the yrast band in the nucleus ^{48}Cr has received a great deal of attention, and the usual explanation in terms of a band crossing is only partly supported by the experimental data. Another important suggestion to explain the observed behavior [3] is the dominance of the seniority $v = 4$ configuration at spin 12^+ [21]. Studies of the spectra of the neighboring nuclei with one proton or neutron either added or removed show energy irregularities along the yrast band. However, it seems to be overseen that this irregularity occurs only in one signature

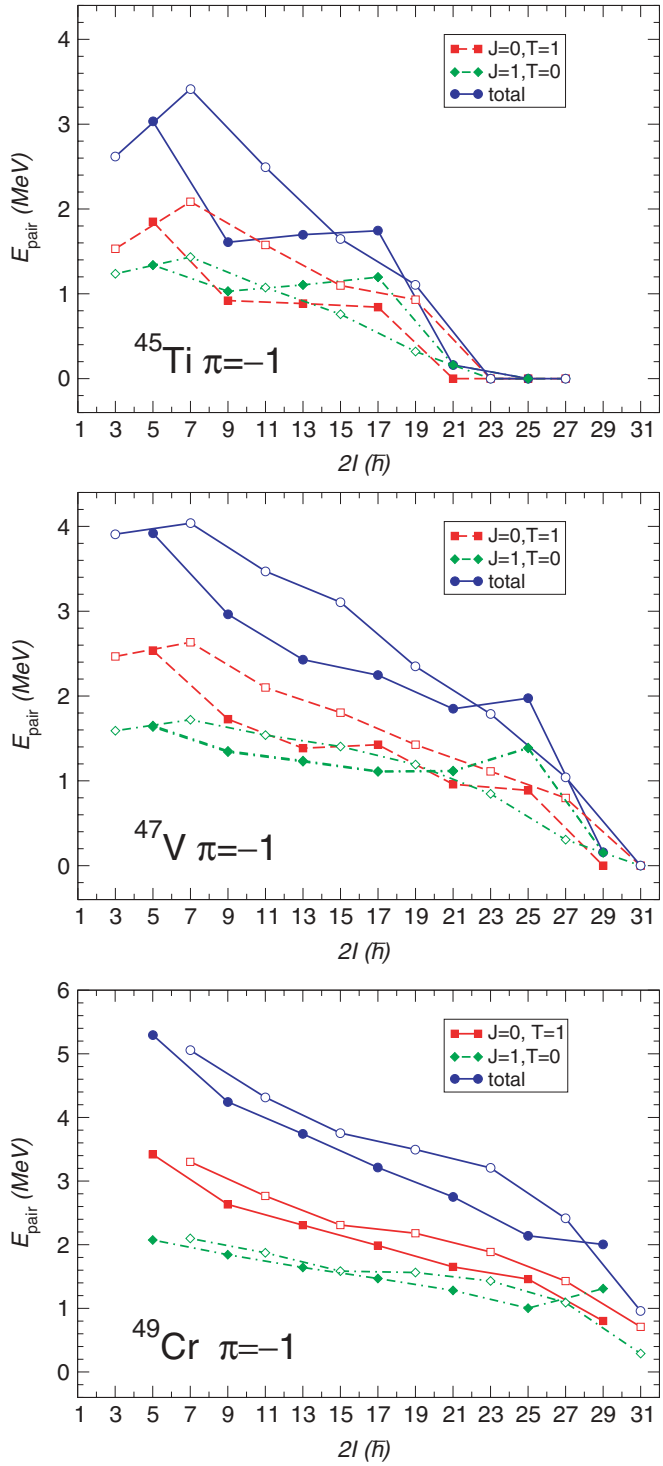

FIG. 16. (Color online) Pairing energy in the ground-state rotational bands of the nuclei ^{45}Ti, ^{47}V, and ^{49}Cr. Filled and open symbols distinguish between different signature bands: $\alpha = +1/2$ and $-1/2$, respectively.

partner, and not in the other. This is seen in Fig. 19, where we show the total angular momentum as a function of the rotational frequency $\hbar\omega = [E_\gamma(I) - E_\gamma(I-2)]/2$. Cameron *et al.* [46] showed the two signatures in ^{49}Cr, but incorrect spin assignments of the high spin states led to a wrong similarity

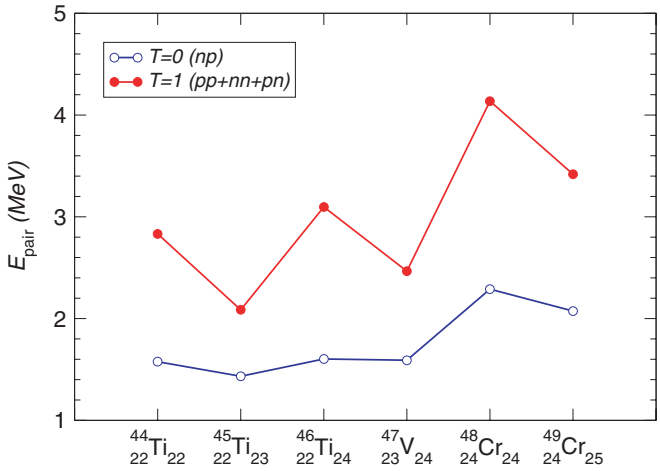

FIG. 17. (Color online) Ground-state pairing energy calculated in the shell model.

between the bands. Martínez-Pinedo *et al.* [44] stated that the backbending behavior would be seen if the energies were plotted as spin vs the rotational frequency. However, they did not discuss that in any detail nor mention the different behavior of the signature bands.

In a backbending plot, Fig. 19(a), we compare the two signature bands in ^{49}Cr with the yrast band in ^{48}Cr. The lowest signature, $\alpha = -1/2$, band in ^{49}Cr (shown as open squares) has a very similar behavior to that of the yrast band in ^{48}Cr with the difference being that the backbend occurs at a lower spin value, $I = 19/2$. The other signature band depends differently on frequency and exhibits no backbending around $I = 10$. The change in the last transition is rather an effect of a band termination [33] than a standard backbend. A similar difference in the signature partners is also observed in ^{47}V, see Fig. 19(b). A difference from ^{49}Cr is that the backbending occurs in the other signature band, $\alpha = +1/2$ (filled squares). Due to the unmeasured $17/2^-$ state in ^{47}V, only the

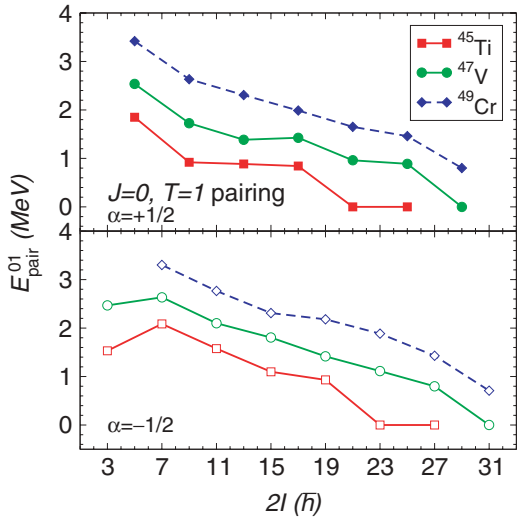

FIG. 18. (Color online) $J = 0$, $T = 1$ pairing energy, calculated in the shell model for odd-A nuclei ^{45}Ti, ^{47}V, and ^{49}Cr.

summed energy of the two transitions, $21/2^- \rightarrow 17/2^-$ and $17/2^- \rightarrow 13/2^-$, is known. If, however, we assume that the excitation energy of this state is close to the value measured in the mirror nucleus ^{47}Cr [47] (as we did in the figure), the backbend is clearly seen. Note that independent of the exact value of the $17/2^-$ energy, this band will show a backbending.

As we saw in previous sections, the sum of the $T = 0$ and $T = 1$ pairing energies (calculated in the shell model and shown in Fig. 16) seems to describe quite well the missing pairing energy in the CNS calculation for odd-A nuclei, see Figs. 9 and 12. When the pairing force is subtracted from the shell model interaction, backbending is reduced, and the two signature bands behave in a similar way. This implies that pairing is the main cause of backbending.

The conclusion is supported by the fact that different values of the pairing strength parameters produce similar results. In our study, we use the normalized form of the pairing interaction [30]. Poves and Martínez-Pinedo used fixed values $G_{01} = -2.95$ MeV and $G_{10} = -4.59$ MeV [26], and the strengths derived for the KB3 interaction are $G_{01} = -4.75$ MeV and

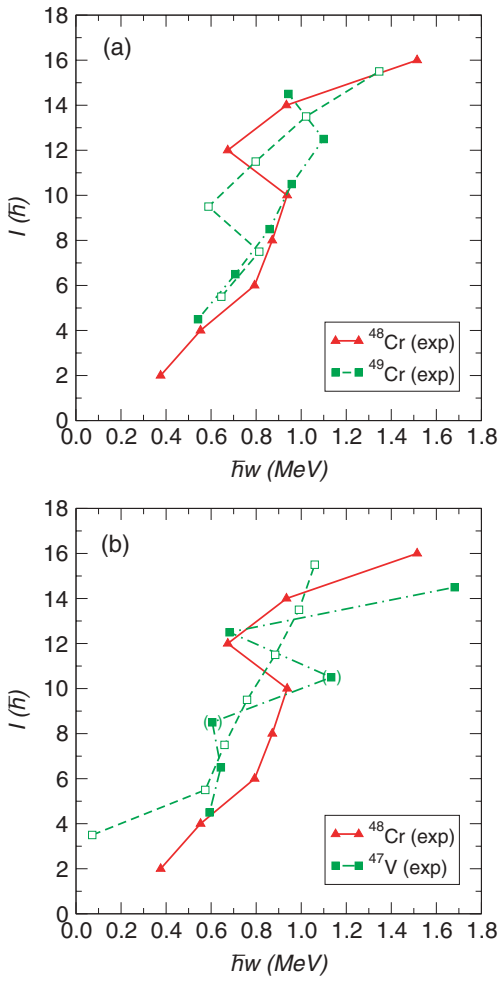

FIG. 19. (Color online) Spin vs rotational frequency in $^{48,49}_{24}$Cr (a) and $^{47}_{23}$V, ^{48}Cr (b). Experimental data are used. For the unknown $17/2^-$ level in ^{47}V, the energy of this level in the mirror nucleus, ^{47}Cr, is assumed [47], and the affected transitions are marked by parentheses.

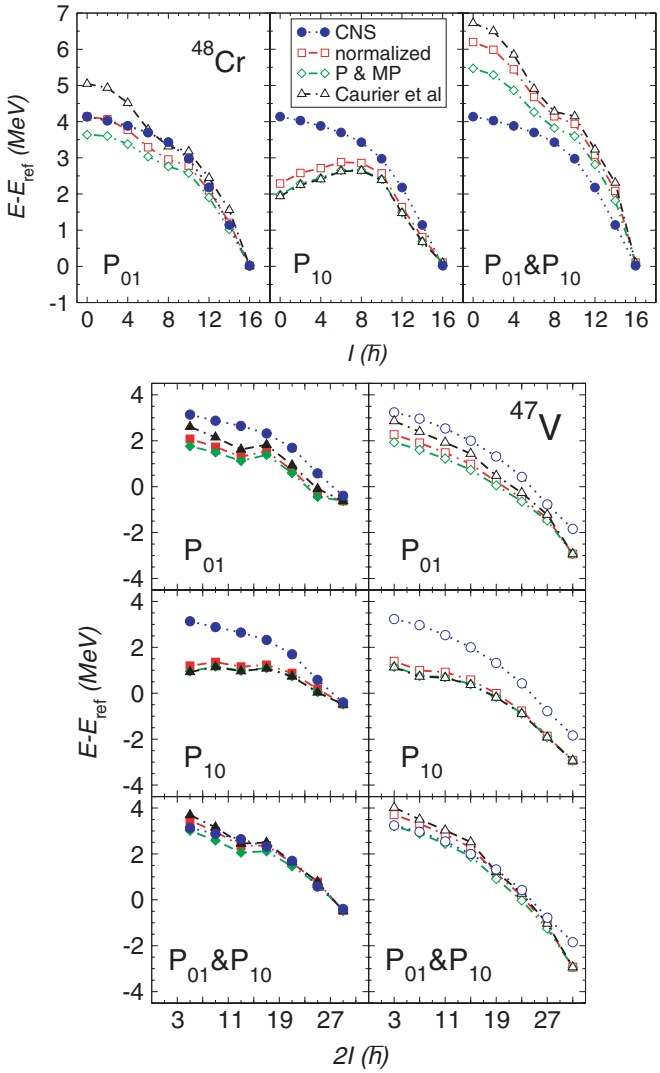

FIG. 20. (Color online) Comparison of CNS and unpaired shell model calculations for three sets of pairing strength: normalized [30], Poves and Martínez-Pinedo (P & MP) [26], and Caurier *et al.* [1]. Plots show ^{48}Cr and ^{47}V. For ^{47}V signature $\alpha = +1/2$ band is in the left panels, and $\alpha = -1/2$, in the right panels. $P_{\rm JT}$ marks which pairing interaction is removed from the Hamiltonian.

$G_{10} = -4.46$ MeV (Table II in Ref. [1]). If we subtract these pairing interactions from the Hamiltonian, the main features, related to the unpaired shell model energies, are not changed: The backbending gets smaller, and the agreement with the CNS results is good for the noted cases (no $T = 1$ pairing for even-even nuclei, and no pairing at all for odd-even nuclei). We illustrate this in Fig. 20 for ^{48}Cr and ^{47}V.

In addition to causing the backbend, pairing increases the signature splitting. A part of the splitting is already present because of a rotational coupling which is well described in the CNS model. Let us discuss how pairing contributes to signature splitting. This also reveals the different backbending behavior in the two signature bands.

In a simple $f_{7/2}$ shell model for the odd-even nuclei ^{45}Ti, ^{47}V, and ^{49}Cr with only $T = 1$ pairing force considered, the pairing energy in both signature partners is the same. However,

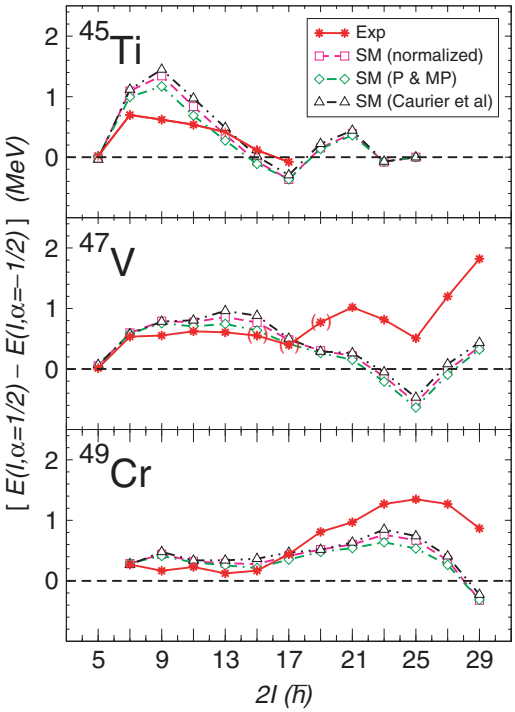

FIG. 21. (Color online) Experimental energy difference between $\alpha = +1/2$ and $\alpha = -1/2$ signature partners (filled symbols) and corresponding differences in total pairing energy (empty symbols).

the values are shifted by 1 unit of angular momentum. For example, the amount of pairing in $5/2^-$ and $7/2^-$ states in ^{49}Cr is the same, because there is no difference in the seniorities of protons and neutrons in these two states: $v_p = 0, v_n = 1$. To gain angular momentum, one needs to break pairs, and it is energetically favored to do that in a similar way in both signature partners. Since the $f_{7/2}$ shell is dominant in a complete shell model calculation, this similarity is seen in the pairing energy of states with the spins I (starting from $I = 5/2$ in the $\alpha = +1/2$ band) and $I + 1$ ($\alpha = -1/2$ band), see Fig. 18. The curve that describes the pairing energy contribution to the $\alpha = -1/2$ band is approximately the same as that for the $\alpha = +1/2$ band, but it is moved to the right by one unit of angular momentum. This $\Delta I = 1$ spin shift gives a contribution to the signature splitting, since the latter is defined as the energy difference between the two signature partner bands calculated at a fixed value of angular momentum.

The summed contribution from the $T = 0$ and $T = 1$ pairings to the signature splitting is studied in Fig. 21 for the considered odd-even nuclei. The figure shows the experimental energy difference between the $\alpha = +1/2$ and $\alpha = -1/2$ bands, and the corresponding differences in the pairing contributions, ΔE_{pair}. The trends agree, although some deviations are expected because the pairing contributions do not account for all effects (e.g., coming from the rotational coupling). The signature splitting from the $T = 0$ pairing behaves smoothly (not separated in the figure), while the irregular behavior comes from the $T = 1$ part. This can be explained to some extent by a trivial shift by one unit of angular momentum between the two signature partners, as discussed above. The change of slope of ΔE_{pair} around $I = 25/2$ in ^{47}V and $I = 17/2$ in ^{49}Cr causes the radically different rotational behavior observed for these nuclei, namely, that one signature band shows a backbending and the other does not.

IV. SUMMARY AND CONCLUSIONS

A comparison was made between the unpaired cranked Nilsson-Strutinsky model and the spherical shell model with the KB3 interaction. It was found that quadrupole properties predicted by the two models agree well. Furthermore, the moment of inertia given by the CNS is close to that from the shell model when either only the $T = 1$ pairing is removed (even-even nuclei) or both $T = 1$ and $T = 0$ pairings are removed (odd-even nuclei). In our study, we used the normalized form of the pairing interaction, but the conclusions do not change if fixed values of the strength parameters are used.

In general, the shell model gives an excellent description of observed signature splittings. It was found that the pairing interaction gives a strong contribution to this splitting. Furthermore, the different spin dependence of the pairing energy for the signature partners in ^{47}V and ^{49}Cr explains why backbending is observed in one but not in the other signature. This behavior comes mainly from the $T = 1$ pairing but is strengthened by the $T = 0$ pairing.

Equilibrium deformations calculated in the CNS model show that some nuclei in the region have noticeably nonaxial shapes with negative γ values, corresponding to rotation around the intermediate axis. These deformations can be traced back to contributions from specific orbitals. The nonaxial deformations are supported by the calculated $B(E2)$ values and spectroscopic quadrupole moments, which agree well with experiment and with those predicted by the shell model. For ^{44}Ti and ^{46}Ti, the contributions from quantum fluctuations around the equilibrium shape led to an improved agreement with experimental $B(E2)$ transition strengths.

The negative-parity band in ^{48}Cr was discussed. This band has the largest calculated negative γ values in this region.

It was also noted that the $B(E2)$ values predicted by the shell model for the unstretched transitions in ^{49}Cr have the expected staggering behavior as a sign of triaxiality.

From this extended comparative study, we conclude that the CNS model gives an adequate description of the quadrupole properties as well as the occupation numbers of the spherical j shells. Furthermore, if the pairing energy calculated from the shell model is added to the unpaired CNS energies, improved agreement to experimental energies is obtained. This is quite a remarkable observation since the shell model with pairing interaction subtracted contains correlations beyond the mean field level, of which CNS is an approximation. It would be most interesting to try to phenomenologically include in the CNS model a pairing force that mimics the pairing energy calculated in the shell model. Such a model, which might be applied to all regions of nuclei, could naturally be tested on the *pf*-shell nuclei studied here.

ACKNOWLEDGMENTS

We thank E. Caurier and F. Nowacki for access to the shell model code ANTOINE [16]. I.R. and S.Å. thank the Swedish Research Council (VR). A.J. thanks GSI (Germany) and Lund Institute of Technology (Sweden), where this work was partially completed, for their support and hospitality.

[1] E. Caurier, G. Martínez-Pinedo, F. Nowacki, A. Poves, and A. P. Zuker, Rev. Mod. Phys. **77**, 427 (2005).
[2] F. Brandolini and C. A. Ur, Phys. Rev. C **71**, 054316 (2005).
[3] F. Brandolini, Eur. Phys. J. A **20**, 139 (2004).
[4] C. A. Ur, Eur. Phys. J. A **20**, 113 (2004).
[5] W. Satuła and R. Wyss, Phys. Rev. Lett. **87**, 052504 (2001).
[6] V. G. Gueorguiev, J. P. Draayer, and C. W. Johnson, Phys. Rev. C **63**, 014318 (2000).
[7] A. Poves, Nucl. Phys. **A731**, 339 (2004); in *Workshop Pingst 2000—Selected Topics on $N = Z$ nuclei, June 2000, Lund, Sweden*, edited by D. Rudolph and M. Hellstrom (Bloms i Lund AB, Lund 2000), p. 138.
[8] A. P. Zuker, J. Retamosa, A. Poves, and E. Caurier, Phys. Rev. C **52**, R1741 (1995).
[9] A. P. Zuker, S. M. Lenzi, G. Martínez-Pinedo, and A. Poves, Phys. Rev. Lett. **89**, 142502 (2002).
[10] P. E. Garrett *et al*., Phys. Rev. Lett. **87**, 132502 (2001).
[11] M. A. Bentley *et al*., Phys. Lett. **B437**, 243 (1998); **B451**, 445E (1999).
[12] C. D. O'Leary *et al*., Phys. Lett. **B525**, 49 (2002).
[13] D. Tonev *et al*., Phys. Rev. C **65**, 034314 (2002).
[14] A. Maj *et al*., Nucl. Phys. **A731**, 319 (2004).
[15] V. M. Strutinsky, Nucl. Phys. **A122**, 1 (1968).
[16] E. Caurier, computer code ANTOINE, CRN, Strasbourg, 1989.
[17] T. Bengtsson and I. Ragnarsson, Nucl. Phys. **A436**, 14 (1985).
[18] A. V. Afanasjev, D. B. Fossan, G. J. Lane, and I. Ragnarsson, Phys. Rep. **322**, 1 (1999).
[19] W. C. Ma *et al*., Phys. Rev. C **65**, 034312 (2002).
[20] W. Satula and R. A. Wyss, Rep. Prog. Phys. **68**, 131 (2005).
[21] A. Juodagalvis, I. Ragnarsson, and S. Åberg, Phys. Lett. **B477**, 66 (2000).
[22] B.-G. Dong and H.-Ch. Guo, Eur. Phys. J. A **17**, 25 (2003).
[23] E. Caurier, J. L. Egido, G. Martínez-Pinedo, A. Poves, J. Retamosa, L. M. Robledo, and A. P. Zuker, Phys. Rev. Lett. **75**, 2466 (1995).
[24] C. E. Svensson *et al*., Phys. Rev. Lett. **85**, 2693 (2000).
[25] A. Poves and A. P. Zuker, Phys. Rep. **70**, 235 (1981).
[26] A. Poves and G. Martínez-Pinedo, Phys. Lett. **B430**, 203 (1998).
[27] A. V. Afanasjev and I. Ragnarsson, Nucl. Phys. **A591**, 387 (1995).
[28] A. Bohr and B. R. Mottelson, *Nuclear Structure* (Benjamin, New York, 1975), Vol. 2.
[29] R. K. Sheline, I. Ragnarsson, S. Åberg, and A. Watt, J. Phys. G: Nucl. Phys. **14**, 1201 (1988).
[30] M. Dufour and A. P. Zuker, Phys. Rev. C **54**, 1641 (1996).
[31] E. Caurier, A. P. Zuker, A. Poves, and G. Martínez-Pinedo, Phys. Rev. C **50**, 225 (1994).
[32] F. Brandolini *et al*., Nucl. Phys. **A642**, 387 (1998).
[33] A. Juodagalvis and S. Åberg, Phys. Lett. **B428**, 227 (1998).
[34] T. Tanaka, K. Iwasawa, and F. Sakata, Phys. Rev. C **58**, 2765 (1998).
[35] K. Hara, Y. Sun, and T. Mizusaki, Phys. Rev. Lett. **83**, 1922 (1999).
[36] T. W. Burrows, Nucl. Data Sheets **68**, 1 (1993).
[37] I. Hamamoto and B. R. Mottelson, Phys. Lett. **B132**, 7 (1983).
[38] C. D. O'Leary, M. A. Bentley, B. A. Brown, D. E. Appelbe, R. A. Bark, D. M. Cullen, S. Ertürk, A. Maj, and A. C. Merchant, Phys. Rev. C **61**, 064314 (2000).
[39] D. Bucurescu *et al*., Phys. Rev. C **67**, 034306 (2003).
[40] S. Schielke, K.-H. Speidel, O. Kenn, J. Leske, N. Gemein, M. Offer, Y. Y. Sharon, L. Zamick, J. Gerber, and P. Maier-Komor, Phys. Lett. **B567**, 153 (2003).
[41] J. A. Cameron and B. Singh, Nucl. Data Sheets **88**, 299 (1999).
[42] P. Bednarczyk *et al*., Eur. Phys. J. A **2**, 157 (1998).
[43] F. Brandolini *et al*., Nucl. Phys. **A693**, 517 (2001).
[44] G. Martínez-Pinedo, A. P. Zuker, A. Poves, and E. Caurier, Phys. Rev. C **55**, 187 (1997).
[45] T. W. Burrows, Nucl. Data Sheets **76**, 191 (1995).
[46] J. A. Cameron, M. A. Bentley, A. M. Bruce, R. A. Cunningham, W. Gelletly, H. G. Price, J. Simpson, D. D. Warner, and A. N. James, Phys. Lett. **B235**, 239 (1990).
[47] J. A. Cameron, M. A. Bentley, A. M. Bruce, R. A. Cunningham, W. Gelletly, H. G. Price, J. Simpson, D. D. Warner, and A. N. James, Phys. Rev. C **49**, 1347 (1994).